Title

Temperature and light reverse the fertility of rice P/TGMS line ostms19 via reactive oxygen species homeostasis.

Journal

Plant Biotechnology Journal, 22(7)

Authors

Zhou, Lei

Mao, Yi-Chen

Yang, Yan-Ming

et al.

Publication Date

2024-07-01

DOI

10.1111/pbi.14322

Peer reviewed

Plant Biotechnology Journal
Open Access

Plant Biotechnology Journal (2024) **22**, pp. 2020–2032 doi: 10.1111/pbi.14322

Temperature and light reverse the fertility of rice P/TGMS line *ostms19* via reactive oxygen species homeostasis

Lei Zhou[1], Yi-Chen Mao[2], Yan-Ming Yang[2], Jun-Jie Wang[2], Xiang Zhong[1], Yu Han[1], Yan-Fei Zhang[1], Qiang-Sheng Shi[3], Xue-hui Huang[2], Blake C. Meyers[4], Jun Zhu[2,*] and Zhong-Nan Yang[1,*]

[1]*Shanghai Engineering Research Center of Plant Germplasm Resources, College of Life Sciences, Shanghai Normal University, Shanghai, China*
[2]*Shanghai Key Laboratory of Plant Molecular Sciences, Shanghai Collaborative Innovation Center of Plant Germplasm Resources Development, College of Life Sciences, Shanghai Normal University, Shanghai, China*
[3]*Jiangxi Yangtze River Economic Zone Research Institute, Jiujiang University, Jiujiang, Jiangxi, China*
[4]*Donald Danforth Plant Science Center, St. Louis, Missouri, USA*

Received 27 November 2023;
revised 30 January 2024;
accepted 17 February 2024.
**Correspondence* (Tel +86 21 64324650; fax +86 21 64324190; email znyang@shnu.edu.cn; Tel +84 21 64322183; fax +86 21 64324190; email zhujun78@shnu.edu.cn)

Keywords: rice, photo/thermo-sensitive genic male sterility, pentatricopeptide repeat (PPR) protein, ROS.

Summary

P/TGMS (Photo/thermo-sensitive genic male sterile) lines are crucial resources for two-line hybrid rice breeding. Previous studies revealed that slow development is a general mechanism for sterility–fertility conversion of P/TGMS in Arabidopsis. However, the difference in P/TGMS genes between rice and Arabidopsis suggests the presence of a distinct P/TGMS mechanism in rice. In this study, we isolated a novel P/TGMS line, *ostms19*, which shows sterility under high-temperature conditions and fertility under low-temperature conditions. *OsTMS19* encodes a novel pentatricopeptide repeat (PPR) protein essential for pollen formation, in which a point mutation GTA(Val) to GCA(Ala) leads to *ostms19* P/TGMS phenotype. It is highly expressed in the tapetum and localized to mitochondria. Under high temperature or long-day photoperiod conditions, excessive ROS accumulation in *ostms19* anthers during pollen mitosis disrupts gene expression and intine formation, causing male sterility. Conversely, under low temperature or short-day photoperiod conditions, ROS can be effectively scavenged in anthers, resulting in fertility restoration. This indicates that ROS homeostasis is critical for fertility conversion. This relationship between ROS homeostasis and fertility conversion has also been observed in other tested rice P/TGMS lines. Therefore, we propose that ROS homeostasis is a general mechanism for the sterility–fertility conversion of rice P/TGMS lines.

Introduction

Hybrid breeding is the most effective and widely applied strategy in crop breeding (Bai *et al.*, 2018). It harnesses hybrid vigour (heterosis) to significantly enhance crop yields by 15%–50% (Tester and Langridge, 2010). Rice is the staple crop for over 50% of the world's population and over 60% of China's population (Yuan, 2014). In China, hybrid rice accounts for 53% of the total rice planting area (Hu *et al.*, 2016). Rice hybrid breeding highly relies on male sterile lines. The discovery of cytoplasmic male sterility (CMS) in the 1970s facilitated the establishment of a three-line breeding system, which is widely employed in rice hybrid production (Si *et al.*, 2011). In the three-line breeding system, the CMS line is crossbred with a maintainer line to maintain male sterility and crossed with a restorer line to produce hybrid seeds (Chen and Liu, 2014). However, the limited germplasm resources of restorer lines and the labour-intensive seed production process have prevented further application (Zhou *et al.*, 2012). The two-line breeding system was developed with the discovery of photo/thermosensitive genic male sterile (P/TGMS) lines. Under high-temperature and long-day photoperiod conditions, the male sterile line can be crossbred with restorer lines for hybrid seed production. Under low-temperature or short-day photoperiod conditions, the fertility of the male sterile line is restored to maintain self-pollinated seeds. P/TGMS lines are controlled by nuclear genetic loci. In the two-line system, almost all rice varieties can serve as restorer lines, effectively utilizing heterosis between different varieties (Zhou *et al.*, 2012; Zhu *et al.*, 2020).

Breeding scientists have identified approximately 15 rice P/TGMS lines due to their important application value (Fan and Zhang, 2018). Of them, *PMS1* and *PMS3/P/TMS12-1* encode small RNAs (Ding *et al.*, 2012; Fan *et al.*, 2016; Zhou *et al.*, 2012); *TMS5* encodes an RNase Z^{S1} protein (Peng *et al.*, 2023, 2024; Zhou *et al.*, 2014); *UGP1* encodes a UDP-glucose pyrophosphorylase (Chen *et al.*, 2007); *TMS10* and *TMS15* encode leucine-rich repeat receptor-like kinases (LRR-RLKs; Han *et al.*, 2023; Yu *et al.*, 2017); *OsTMS18* encodes a glucose-methanol-choline (GMC) oxidoreductase (Zhang *et al.*, 2022); and *OsMS1* encodes a histone binding protein (Wu *et al.*, 2022). The investigation of these genes has revealed the mechanism of P/TGMS at the genetic level. A pollen grain is a specialized plant cell. The essence of P/TGMS is whether functional pollen can be formed (Zhu *et al.*, 2020). Recent studies of Arabidopsis P/TGMS lines revealed the cellular mechanism underlying sterility and fertility restoration of P/TGMS lines. P/TGMS genes are involved in the cell wall transition from microsporocyte to mature pollen. Mutations in these genes lead to defective pollen wall formation in P/TGMS lines, leading to pollen rupture and male sterility. Slow

development under low-temperature or short-day photoperiod conditions is a common mechanism that is utilized to restore their fertility (Zhang *et al*., 2020; Zhu *et al*., 2020). Slow development reduces the requirement for wall protection so that microspores can develop into functional pollen (Shi *et al*., 2021; Wang *et al*., 2022).

The reproductive development process in rice and Arabidopsis is highly conserved. However, the reported P/TGMS genes in rice are quite different from those reported in Arabidopsis. Knockout of *TMS5* in rice leads to the TGMS phenotype, whereas the mutant of its homologous gene *AtTrz1* in Arabidopsis does not show any obvious phenotype (Canino *et al*., 2009; Zhou *et al*., 2014). Additionally, a single base mutation in *OsTMS18* results in the TGMS phenotype in rice. The knockout allele of *AtTMS18* in Arabidopsis exhibits normal fertility at normal temperature (24 °C) and only partial sterility under high-temperature stress (28 °C) (Zhang *et al*., 2022). These observations suggest that rice has other P/TGMS mechanisms in addition to slow development.

Reactive oxygen species (ROSs) play a dual role in plants, acting as both toxic byproducts of aerobic metabolism and key regulatory factors in growth, development and defence pathways (Mittler *et al*., 2004). Redox homeostasis plays an important role in the normal growth and development of plants. The generation and scavenging of ROSs are crucial for maintaining redox homeostasis (Xie *et al*., 2022). In this study, we reported a novel rice P/TGMS line, *ostms19*. The *OsTMS19* gene encodes a mitochondrial-targeted PPR protein. Through investigation of *OsTMS19*, we revealed that environmental factors such as temperature and photoperiod influence the male sterility and fertility of *ostms19* through ROS homeostasis. Further evidence indicated that ROS homeostasis is likely a general mechanism of the sterility–fertility transition of rice P/TGMS lines.

Results

ostms19 is a new TGMS line

The rice TGMS line *ostms19* was obtained utilizing EMS mutagenesis of ZH11 (*Oryza sativa* ssp. *japonica*) as described in a previous study (Zhang *et al*., 2022). It exhibited male sterility under high temperatures (>29 °C) (Figure 1b) but fertility was restored under low temperatures (<24 °C) (Figure 1c). Under high temperatures, the *ostms19* anther was obviously smaller than that of the wild type. Potassium iodide staining showed that most pollen was shrunken, while the remaining pollen was hollow without staining (Figure 1g–i). Under low temperatures, the anthers of *ostms19* became plump and contained abundant mature pollen with potassium iodide staining (Figure 1j–l). To assess the TGMS trait of *ostms19*, batches of *ostms19*, *tms5*, *ostms15* and *ostms18* seeds were germinated once a week and then transplanted into paddy fields from May to August during 2020–2022 as previously described (Han *et al*., 2023). The booting time of each batch and the corresponding average temperature were recorded. Based on the field performance from 2020 to 2022, the selfing seed-setting rate of *ostms19* was higher than that of *tms15* and lower than that of *tms5* and *tms18* under high-temperature conditions (>29 °C) (Figure 1m). Under low-temperature conditions (<24 °C), the fertility of *ostms19* was significantly restored (Figure 1n). These results suggest that *ostms19* exhibits a typical P/TGMS trait during the normal planting season.

A point mutation in the *OsTMS19* gene leads to the TGMS phenotype

When *ostms19* was crossed with the wild type, the F_1 generation exhibited normal fertility. In the self-pollinated F_2 population, fertile and sterile plants in the F_2 population segregated at 174 : 59 ($\chi^2 = 0.0128$ for 3 : 1, $P > 0.05$), indicating that the TGMS phenotype of *ostms19* is controlled by a single recessive Mendelian locus. To identify the candidate gene responsible for *ostms19*, we conducted bulked segregant analysis (BSA) using this F_2 population. The results showed a point mutation, with thymine (T) being replaced by cytosine (C), in the unique exon of the *LOC_Os02g21580* gene, resulting in a GTA (Val) to GCA (Ala) substitution in the *ostms19* mutant (Figure 2a). *LOC_Os02g21580* encodes a pentatricopeptide repeat (PPR) protein. In rice, the PPR family has 491 members (Chen *et al*., 2018). To confirm the candidate gene, a genomic fragment including the coding sequence of *LOC_Os02g21580* and its upstream promoter sequence was cloned using wild-type DNA as a template and then stably transformed into the *ostms19* mutant. A total of 28 transgenic lines were obtained, all of which exhibited normal fertility under high temperatures (Figure 2b). This confirms that the mutation in *LOC_Os02g21580* is responsible for the *ostms19* phenotype. Quantitative real-time PCR analysis showed that the expression of *OsTMS19* in anthers was significantly higher than that in other tissues, with the highest expression observed during the mitosis and pollen maturation stages (Figure 2c). Further *in situ*, hybridization showed that the *OsTMS19* transcripts were highly expressed in the tapetum and microspores at stages 10 and 11 of anther development (Figure 2d–k). To investigate the expression pattern of the OSTMS19 protein, we fused the genomic DNA sequences of OsTMS19 to GFP driven by its native promoter. This construct also complemented the male-sterile phenotype of *ostms19* under high temperatures (Figure S1a). However, GFP signals were not observed in these transgenic lines (Figure S1b–e). Therefore, we performed immunohistochemistry using a GFP antibody to determine the distribution of the OsTMS19–GFP fusion protein in anthers. The results showed that the OsTMS19 protein primarily accumulated in tapetum cells and microspores at stages 10–11 (Figure 2l–q).

OsTMS19 is located in mitochondria and is essential for normal rice growth and development

In terrestrial plants, PPR family proteins are predominantly found in semiautonomous organelles such as mitochondria or chloroplasts (Colcombet *et al*., 2013). To precisely determine the subcellular localization of OsTMS19 in rice cells, the full-length cDNA of OsTMS19 was fused with GFP driven by the 35S promoter, and the fusion protein was transiently expressed in rice protoplasts. To distinguish mitochondria from the cytoplasm, we used the mitochondria-specific dye MitoTracker Red CMXRos. The results showed a significant overlap between the green fluorescence signal of GFP and the red signal of MitoTracker, indicating that the OsTMS19 protein is localized in mitochondria (Figure 3a). We further analysed the activities of electron transport chain (ETC) complexes of *ostms19*. The results showed that the activities of mitochondrial complexes I, III, IV and V were obviously reduced in the *ostms19* mutant compared with ZH11 under high temperatures (Figure 3b), which indicated that the mitochondrial function was impaired in *ostms19*.

OsTMS19 contains 12 PPR motifs, including three long-type and nine short-type motifs. The Val to Ala substitution occurs in

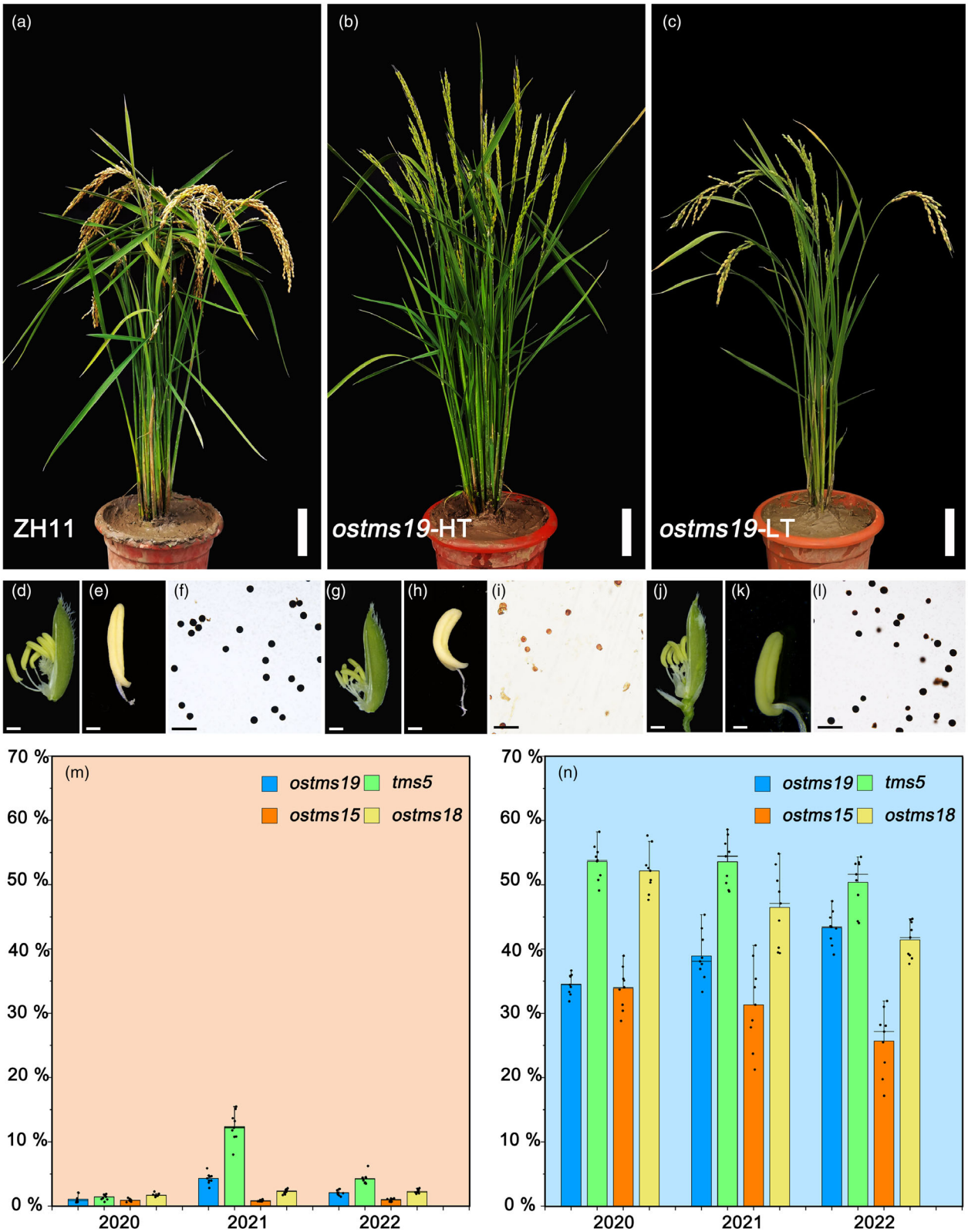

Figure 1 TGMS traits of *ostms19*. The WT plant (a) and *ostms19* mutant after the booting stage under high temperature (b) and low temperature (c). HT, high temperature (over 29 °C); LT, low temperature (below 24 °C). Bar = 10 cm. (d, g, j) The spikelets of the WT plant and *ostms19* mutant under different temperatures after removing the palea. (e, h, k) The anthers of WT plants and *ostms19* mutants under different temperatures. (f, i, l) I_2/KI staining of anthers in WT plants and *ostms19* plants under different temperatures. Bars = 200 μm. (m, n) The left Y-axis represents the seed setting rates of different batches of *ostms19*, *ostms15*, *ostms18* and *tms5* under the high-temperature season (m) and low-temperature season (n) in 2020, 2021 and 2022. The panicles were divided into three groups (n = 3). Each group had six panicles. The values are the mean ± SE.

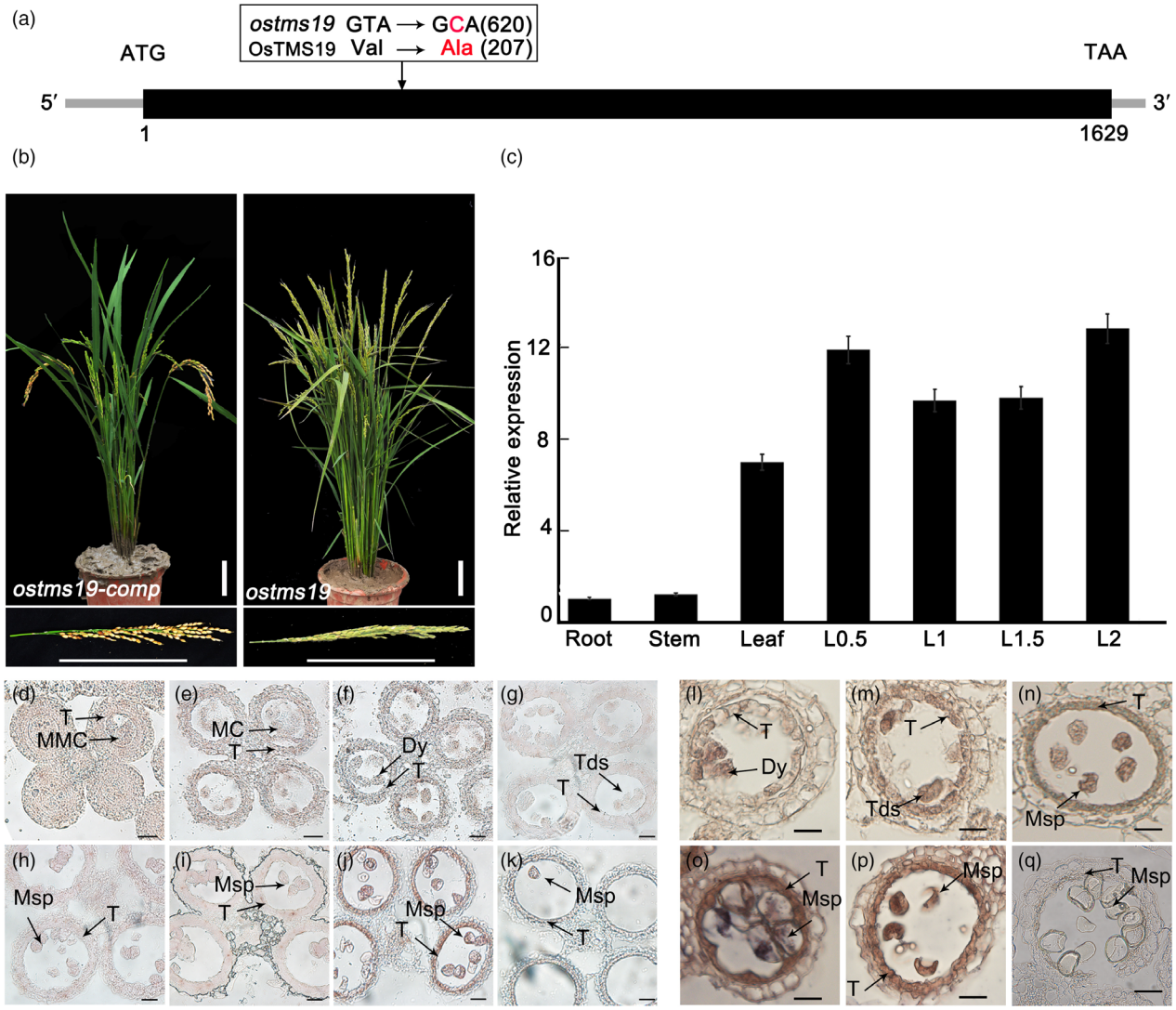

Figure 2 *OsTMS19* encodes a PPR in which a point mutation leads to the TGMS phenotype of *ostms19*. (a) Gene structure of the *OsTMS19* locus. The black arrow indicates the mutation site, and the red font represents the mutant base (position 620) and mutant amino acid (position 207) in *ostms19*. The black box indicates the exon. (b) The *ostms19-com* plant and panicle after the booting stage under high temperatures; *ostms19* plant and panicle were used as controls. Bars = 10 cm. (c) qRT–PCR analysis of *OsTMS19*. The *OsACTIN* gene served as the reference. Pa (palea), Le (lemma), Anther L1, anther length 0.5 mm; Anther L2, anther length 1 mm; Anther L1.5, anther length 1.5 mm; Anther L2, anther length 2 mm. Data are shown as the mean ± SD (n = 3). *In situ* hybridization of *OsTMS19* transcripts in WT anthers at stage 6 (d), stage 7 (e), stage 8a (f), stage 8b (g), stage 9 (h), stage 10 (i) and stage 11 (j) with an *OsTMS19* antisense probe. The anthers at stage 11 (k) hybridized to an *OsTMS19* sense probe. Bars = 50 μm. (l–q) Immunolocalization of the fusion protein OsTMS19–GFP (brown) in anther sections of a male-sterile transgenic line at stage 8a (l), stage 8b (m), stage 9 (n), stage 10 (o) and stage 11 (p) probed with a commercial GFP antibody. ZH11 at stage 10 (q) was used as a negative control. Bars = 50 μm.

the fifth PPR motif in *ostms19* (Figure 3c). To further understand the function of this gene, we employed CRISPR–Cas9 technology to generate different alleles of *OsTMS19*. A total of eight independent CRISPR lines were obtained. These lines exhibited 1–2 amino acid substitutions (lines 1, 3, 4, 6, 8), 1–5 amino acid deletions (lines 1, 2, 4, 5, 6, 7) and two amino acid insertions (line 8) (Figure 3d). Among them, *ostms19-7* displayed the most serious alteration with a deletion of five amino acids. This line exhibited complete male sterility without any fertility restoration even under low temperatures (Figure 3g,h). The remaining seven lines maintained fertility under high temperatures, suggesting that these mutations do not affect their function in pollen formation. Of all the CRISPR–Cas9 transgenic lines, we failed to obtain lines with premature termination or frameshift mutations.

In addition, the height of *ostms19* was significantly lower than that of ZH11 (Figure S2). *OsTMS19* is likely important for embryogenesis and normal growth. Evolutionary analysis revealed that the homologues of the OsTMS19 protein are exclusively found in monocotyledonous plants (Figure S3).

Efficient ROS scavenging is the key to restoring the fertility of *ostms19* under low-temperature conditions

Mitochondrial dysfunction is frequently associated with oxidative bursts (Wan *et al.*, 2007; Wu *et al.*, 2024). We employed histochemical staining with nitroblue tetrazolium (NBT) to determine ROS accumulation during anther development (Zheng *et al.*, 2019). In the wild type, the ROS signals were obviously detected during stages 7 to 9. During stages 10–11, microspores

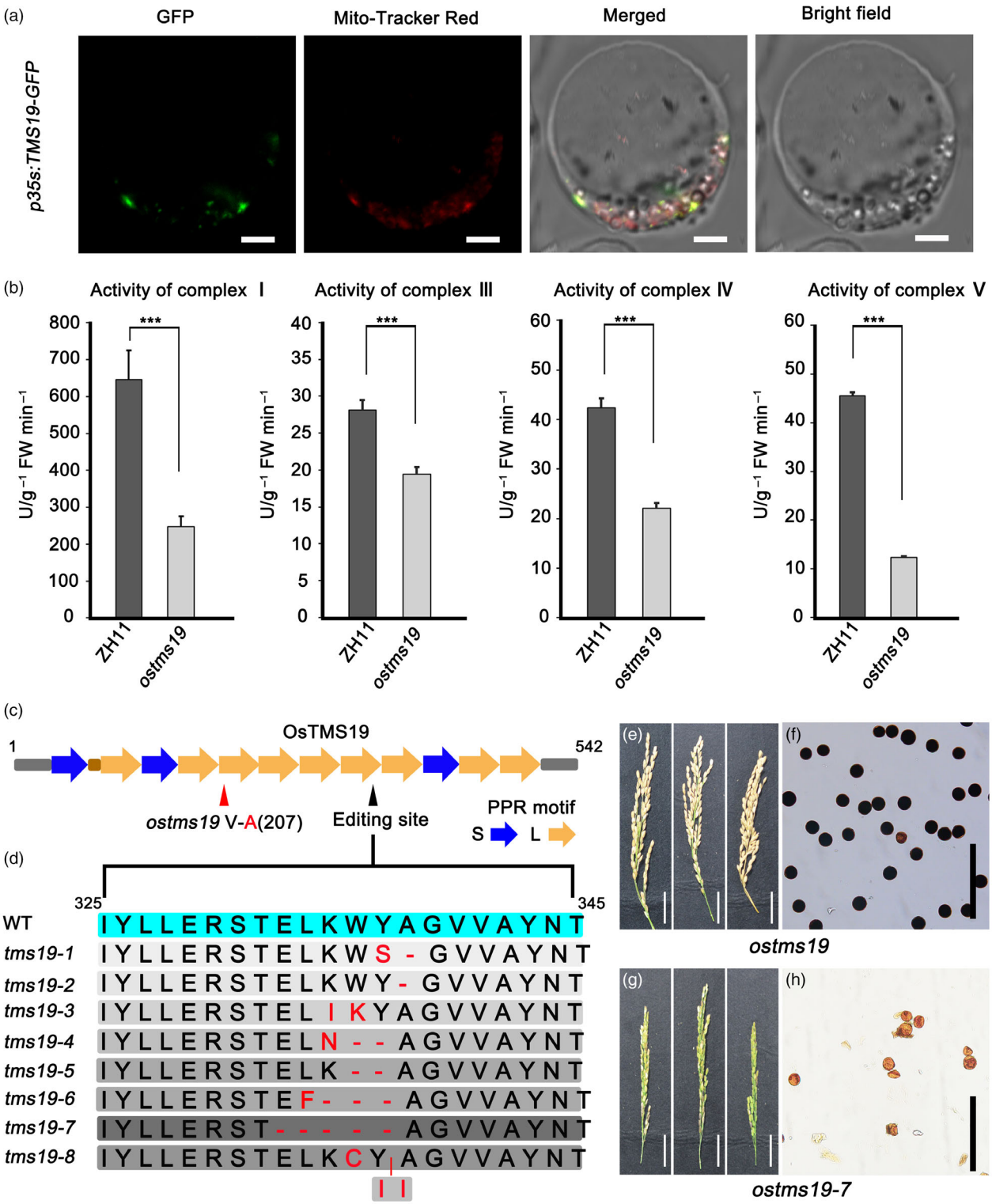

Figure 3 Knockout of mitochondrion-localized *OsTMS19* led to complete male sterility. (a) Subcellular localization of OsTMS19. Transient expression of *p35s::OsTMS19-GFP* in rice protoplasts. Mito-Tracker Red CMXRos was used as a mitochondria indicator. Bars = 5 μm. (b) Detection of the activities in mitochondrial ETC complexes I, III, IV and V in fresh leaves of ZH11 and *ostms19* under high temperatures. *0.01 < *P* < 0.05. **$P < 0.01$. ***$P \leq 0.001$. Error bars indicate ±SD. Each reaction represents three biological replicates. (c) Schematic diagram of the targeted sites of CRISPR–Cas9 in the *OsTMS19* locus. The numbers indicate the distance to the first encoding amino acid. (d) The mutation sites in the OsTMS19 amino acid sequence of the gene editing plant. Amino acid substitution from WT (black) to mutants (red). The mutation site in *ostms19* is marked with a black arrow. (e–h) Panicle phenotypes and I_2/KI staining of the pollen in *ostms19* (e, f) and *ostms19-7* (g, h) under low temperatures. Bars = 2 cm (e, g). Bars = 200 μm (f, h).

undergo PM I (pollen mitosis I) and PM II (pollen mitosis II) and begin to synthesize the pollen intine wall. During this period, the ROS signal was almost undetectable (Figure 4a). It is likely that PM I and PM II are sensitive to ROS, and rice itself has the ability to scavenge the produced ROS. Under high temperatures, strong ROS signals were detected at all stages of anther development, including PM I and PM II in *ostms19* (Figure 4b). Under low temperatures, the content of ROS in the anthers of *ostms19* at stages 10–11 significantly decreased (Figure 4c). We used ImageJ to analyse the relative content of ROS in the above sections of *ostms19* anthers at high and low temperatures. The results showed that under high temperatures, the anthers of *ostms19* exhibited a significant increase in ROS content at stages 10–11 but returned to a level comparable to that of the wild type under low temperatures (Figure 4d). H_2DCF-DA (2,7-dichlorodihydrofluorescein diacetate) can react with ROS to generate high fluorescence DCF (Wu *et al.*, 2023). We used an H_2DCF-DA solution to stain the anthers of *ostms19* under high- and low-temperature conditions, which also showed similar results (Figure 4e). ROS accumulation was consistent with the fertility of *ostms19* under different temperature conditions.

The inner wall intine is defective under high temperature in *ostms19*

To evaluate the impact of excessive ROS in *ostms19*, we conducted cytological analysis to compare anther development and pollen formation between *ostms19* and ZH11. Under high temperature, numerous collapsed pollen grains within *ostms19* locules were observed (Figure S4d–f). Under low temperature, *ostms19* pollen exhibited a round and plump shape (Figure S4g–i), resembling that of the wild type (Figure S4a–c). We further stained the pollen exine and intine with basic fuchsin and fluorescent brightener-28, respectively (Jia *et al.*, 2021; Yang *et al.*, 2022). The exine (red signal) and intine (green signal) of the wild-type pollen were tightly adhered, forming a concentric pattern (Figure 5a). In *ostms19*, although both the exine and intine could be stained, the intine layer exhibited irregular wrinkled and curled morphology under high temperature (Figure 5a). The statistical analysis revealed that 10% of *ostms19* microspores exhibited an absent intine layer, 43% collapsed, and the remaining 47% had wrinkled intine under high temperature (Figure S5). Under low temperature, the deposition pattern of the exine and intine of the *ostms19* microspores was similar to that of the wild type (Figure 5a). Several genes have been reported to be involved in the synthesis and transportation of sporopollenin precursors in rice (Han *et al.*, 2021). The expression of these genes did not show significant differences between wild type and *ostms19* under high temperature (Figure 5b). TEM showed that the exine structure was not affected in the *ostms19* mutant (Figure S6). These results suggest that the male sterility of *ostms19* under high temperature is not related to the exine, while the defective intine may be the direct cause of its male sterility. It was reported that an increase in ROS accumulation can damage microspore nuclear DNA, leading to microspore abortion (Jiang *et al.*, 2022; Xue *et al.*, 2020). We performed the comet assay using pollen grains collected from the *ostms19* mutant

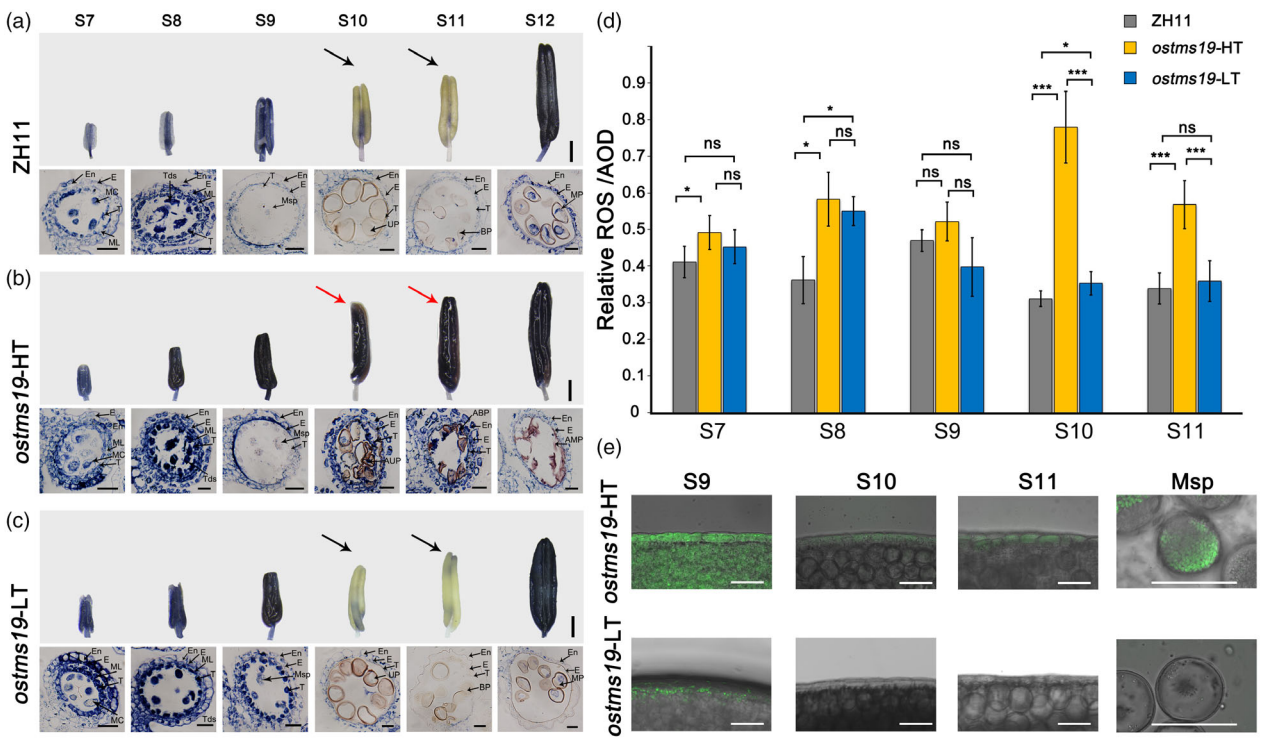

Figure 4 Analyses of ROS in ZH11, *ostms19*(HT) and *ostms19*(LT) anthers. NBT staining of superoxide anion production (up) and sections (below) in ZH11 (a), *ostms19* (HT) (b) and *ostms19* (LT) (c) anthers from stage 7 to stage 12. Stage 10 and stage 11 are highlighted by arrows with different colours. Bars = 200 μm (top). Bars = 200 μm (below). (d) Relative quantification of ROS levels in ZH11 *ostms19* (HT) and *ostms19* (LT) anthers from stage 7 to 11 based on NBT staining of ROS. *$0.01 < P < 0.05$. ***$P \leq 0.001$. Error bars indicate ±SD. Each reaction represents three biological replicates. (e) H_2DCF-DA staining analysis of ROS in *ostms19* (HT) and *ostms19* (LT) anthers and pollens. Bars = 50 μm.

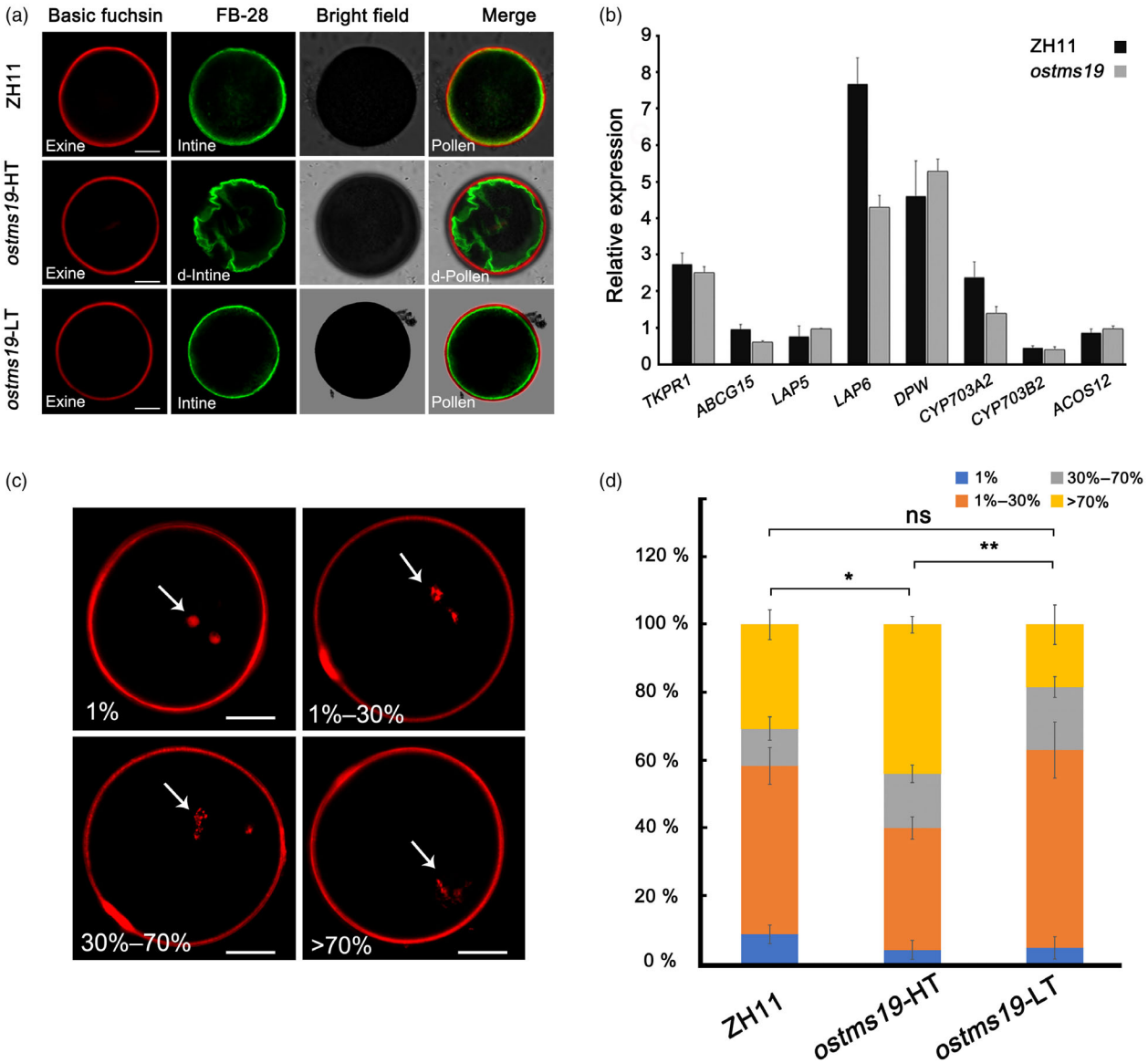

Figure 5 Pollen wall staining and comet assay of *ostms19* pollen at different temperatures. (a) The exine (red) and intine (green) stained by basic fuchsin and FB-28, respectively, in ZH11, *ostms19* (HT) and *ostms19* (LT). (b) The expression of genes related to exine formation (*TKPR1*, *ABCG15*, *LAP5*, *LAP6*, *DPW*, *CYP703A2*, *CYP703B2* and *ACOS12*) in ZH11 and *ostms19* under high temperature. Data are shown as the mean ± SD (n = 3). (c) Representative images of four arbitrarily determined classes of DNA damage: nuclei with little or no DNA in the tails were defined as 1%, less than 30% DNA in tails as 1%–30%, 30%–70% DNA in tails as 30%–70%, and almost all the DNA in tails as >70%. (d) Frequency distribution of the classes of DNA damage in ZH11, *ostms19*(HT) and *ostms19*(LT). *0.01 < P < 0.05. **P < 0.01. The data represent the means ± SDs (n = 3).

under different temperatures to evaluate DNA damage in pollen nuclei. Under high temperature, the extended comet tail of DNA damage in *ostms19* pollen nuclei was significantly higher than that in ZH11 pollen, while under low temperature, the DNA damage in *ostms19* pollen nuclei decreased to the wild-type level (Figure 5c,d). The effect of temperature was closely related to the accumulation of ROS under different temperatures, which impacted the fertility of *ostms19*. This indicates that ROS play an important role in the TGMS trait of *ostms19*. Intine is genetically controlled by the microspore (gametophyte) itself. Genetic analysis indicates that *OsTMS19* plays a role as a sporophytic gene. It is likely that ROS produced in sporophytic tissue tapetum were distributed into microspores, affecting their gene expression and intine formation.

ROS accumulate under high temperature and are scavenged under low temperature in other P/TGMS lines

ROS homeostasis is critical for *ostms19* fertility. We analysed whether this ROS homeostasis is also present in other P/TGMS lines, including *tms5*, *ostms15* and *ostms18*. NBT staining showed that ROS were also significantly accumulated in anthers at stages 10–11 in *tms5*, *ostms15* and *ostms18* under high temperature (Figure 6a–c). Under low temperature, the ROS in the anthers of these stages was efficiently decreased, similar to the wild type (Figure 6d–f). These results suggested that ROS homeostasis is also critical for the fertility conversion of these P/TGMS lines. In *tms5*, the knockout of an RNase Z^{S1} protein leads to the TGMS phenotype (Zhou *et al.*, 2014). *ostms15* is a P/TGMS line with

defective tapetal initiation (Han *et al.*, 2023). *ostms18* exhibits a defective exine layer (Zhang *et al.*, 2022). These P/TGMS genes play different roles in pollen formation. This suggests that *OsTMS19* and other P/TGMS genes are indirectly related to ROS accumulation.

Plants under a high temperature/long-day photoperiod produce more ROS than those under a low temperature/short-day photoperiod

Redox homeostasis plays an important role in plant growth and development, which relies on ROS production and scavenging (Gechev *et al.*, 2006; Mittler *et al.*, 2004). In the wild type, the anthers at stages 10–11 maintained low levels of ROS even under high temperature, indicating their ability to scavenge ROS during these stages. In the P/TGMS lines, such as *tms5*, *ostms15*, *ostms18* and *ostms19*, the excessive ROS accumulation under high temperature suggested that mutations in these genes indirectly promote ROS production, which the plants themselves failed to scavenge. However, under low temperature, the ROS in these P/TGMS lines were effectively cleared, indicating that temperature could significantly impact ROS accumulation. Since P/TGMS lines show male sterility under high temperature or long-day photoperiod, we further analysed whether these environmental conditions facilitate ROS production. We used H_2DCF-DA to stain ZH11 anthers and mature pollen. Under high temperature, significant ROS fluorescence signals were detected in both anthers and mature pollen. However, the ROS signal was barely detectable in these tissues under low temperature (Figure 7a,b). Under a long-day photoperiod, ROS fluorescence signals also accumulated in anthers and mature pollen but were significantly reduced under a short-day photoperiod (Figure 7c,d). We further analysed the H_2O_2 content in ZH11 anthers under different temperature and photoperiod conditions using a quantitative analysis kit. The results showed that the H_2O_2 content in anthers under HT/LD conditions was significantly higher than that under LT/SD conditions (Figure 7e). These results revealed that HT/LD conditions facilitate ROS production in wild-type anthers.

Discussion

ROS homeostasis is the key to fertility conversion in rice P/TGMS lines

During rice anther development, the microspores in PM I and PM II are sensitive to ROS, which need to be maintained at a low level to ensure microspore development into mature pollen (Chaturvedi *et al.*, 2021; Zhang *et al.*, 2011). In this study, we identified a new rice P/TGMS line, *ostms19* (Figure 1b,c). Under high temperature conditions, *ostms19* exhibited male sterility due to excessive ROS accumulation during the PM I and PM II stages (Figure 4b). However, under low-temperature conditions, the production of ROS was reduced, leading to fertility restoration (Figure 4c). Thus, ROS homeostasis is crucial for fertility restoration in *ostms19*. Other P/TGMS lines, including *tms5*, *ostms15* and *ostms18*, all showed ROS accumulation under high temperature and ROS scavenging under low temperature (Figure 6). Therefore, ROS homeostasis is a general mechanism of rice P/TGMS lines. Redox homeostasis plays an important role in plant growth and development, which relies on ROS

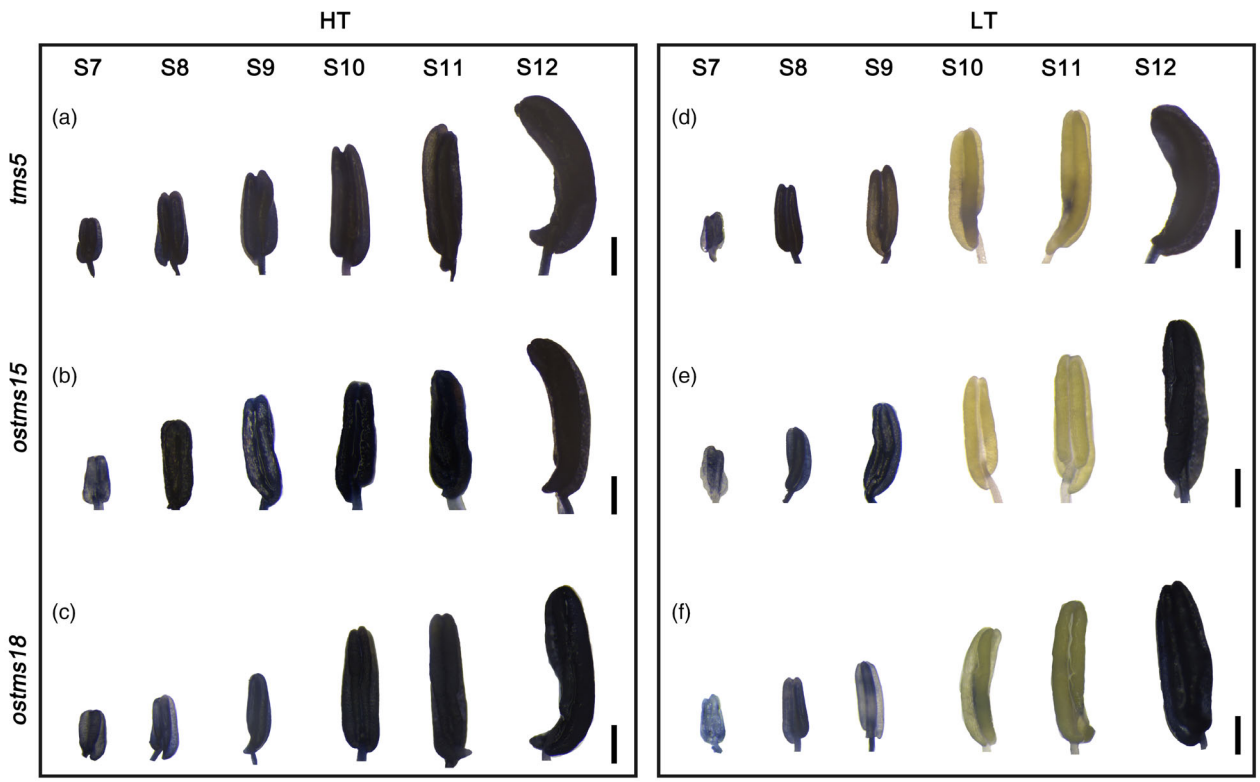

Figure 6 Analyses of ROS in *tms5*, *ostms15* and *ostms18* anthers under different temperature conditions. NBT staining of superoxide anion production in *tms5* (a), *ostms15* (b) *and ostms18* (c) anthers at HT from stage 7 to stage 12. NBT staining of superoxide anion production in *tms5* (d), *ostms15* (e) *and ostms18* (f) anthers at LT from stage 7 to stage 12. HT, high temperature (over 29 °C); LT, low temperature (below 24 °C). Bars = 500 μm.

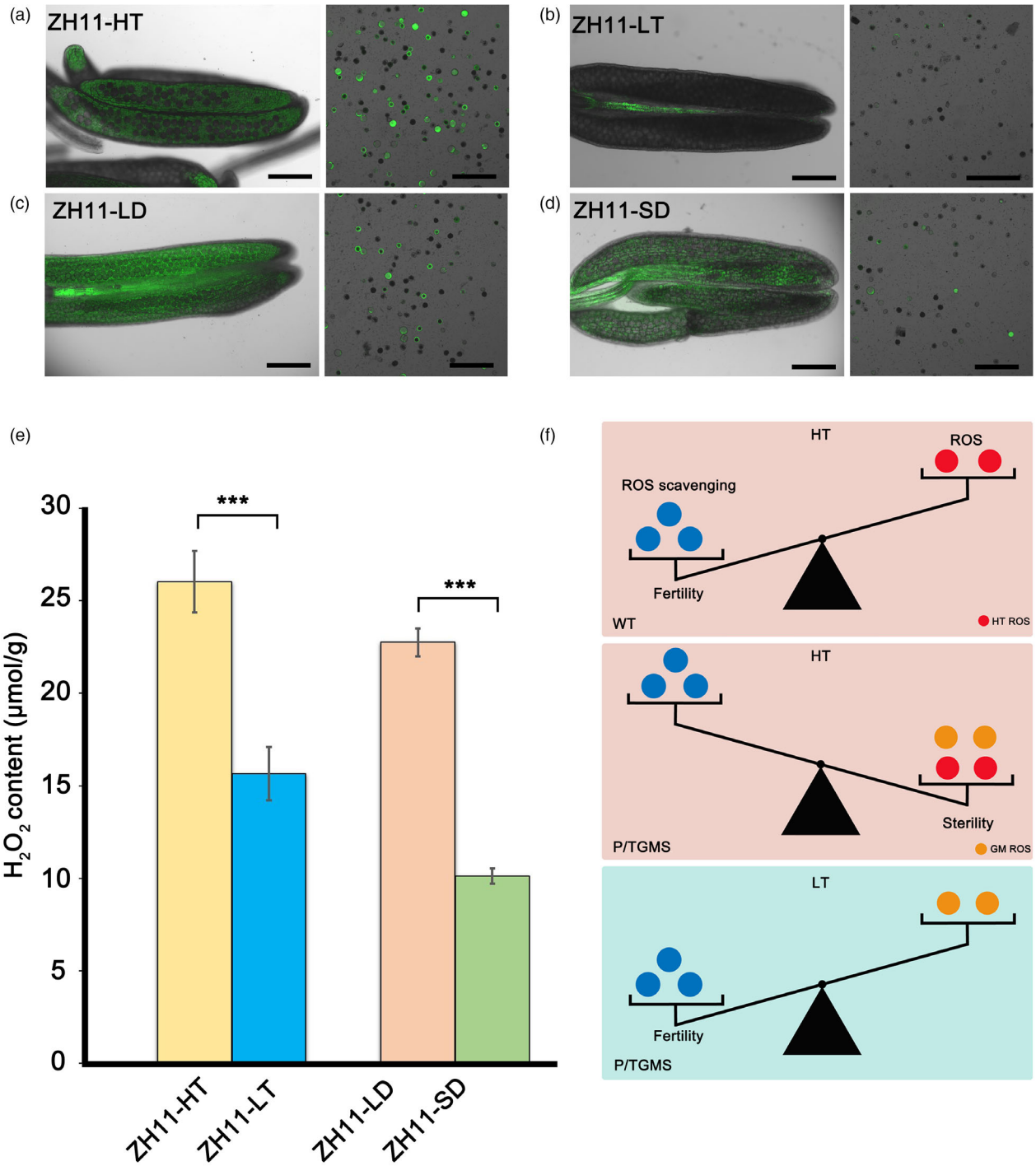

Figure 7 Analyses of ROS in ZH11 anthers under different temperature and photoperiod conditions. H_2DCF-DA staining analysis of ROS in ZH11 anthers and pollen at high temperature (a), low temperature (b), long-day photoperiod (c), and short-day photoperiod (d). (e) Content of H_2O_2 in ZH11 anthers under different temperature and photoperiod conditions. HT, high temperature (over 29 °C); LT, low temperature (below 24 °C); LD, long-day photoperiod (8 h light, 2055 μmol m^{-2} s^{-1}, 28 °C); SD, short-day photoperiod (4 h light, 2055 μmol m^{-2} s^{-1}, 28 °C). Bars = 200 μm. *0.01 < P < 0.05. **P < 0.01. ***$P \leq 0.001$. Error bars indicate ±SD. Each reaction represents three biological replicates. (f) Light and temperature control the fertility transition of P/TGMS by affecting ROS homeostasis. GM, P/TGMS genetic mutations.

production and scavenging (Gechev *et al.*, 2006; Mittler *et al.*, 2004). In non-photosynthetic plant tissues, mitochondria are the main sources of ROS (Waszczak *et al.*, 2018; Willekens *et al.*, 1997). *OsTMS19* encodes a PPR protein localized in mitochondria and is highly expressed in the tapetum. In *ostms19*, the mutation in the PPR protein led to abnormal mitochondrial function (Figure 3b), which resulted in a large amount of ROS being produced under high temperature (Figure 4). It is likely that the mutation in *OsTMS19* directly leads to excessive ROS accumulation in *ostms19*. For *tms5*, the microspore mother cells (MMCs)

were impaired leading to pollen abortion (Zhou *et al.*, 2014). In *ostms15* and *ostms18*, their outer pollen wall exine is defective (Han *et al.*, 2023; Zhang *et al.*, 2022). The gene loci and their functions for pollen development are different. It is likely that the genetic mutations of these genes are indirectly related to ROS production in these P/TGMS lines.

Based on the ROS accumulation in multiple P/TGMS lines under different conditions, we propose that the ROS homeostasis induced by temperature/photoperiod and genetic mutations is closely correlated with the fertility of P/TGMS lines. Under high temperature, the wild type could scavenge the produced ROS, and the plant showed fertility. Gene mutations in P/TGMS lines may cause extra ROS accumulation in anthers. In this case, the P/TGMS lines failed to completely scavenge ROS and showed male sterility. Under low temperature, the plant itself produced less ROS. In this case, P/TGMS lines scavenged ROS and showed fertility (Figure 7f).

ROS generated by sporophytes affect microspore development and intine formation

During anther development, the 'transition period' is crucial for microspore development and pollen formation (Shi *et al.*, 2021; Yao *et al.*, 2022). Many reported P/TGMS genes are directly or indirectly involved in cell wall transition (Dong *et al.*, 2005; Xu *et al.*, 2021; Zhu *et al.*, 2020). Typically, intine formation is controlled by gametophytes. In maize, elevated levels of ROS damage the nuclear DNA of microspores, resulting in male sterility (Jiang *et al.*, 2022). In this study, under high-temperature conditions, *ostms19* exhibited abnormal pollen intine formation (Figure 5a), accompanied by degradation of microspore nuclei (Figure 5c). This suggests that excessive ROS affect gametophyte development. Genetic analysis indicated that *OsTMS19* is a sporophytic gene mainly expressed in the tapetum during anther development (Figure 2). Due to their diffusion ability, the ROS generated by sporophyte tissues can affect the development of gametophyte microspores, resulting in a male sterility phenotype. Previous studies have identified multiple P/TGMS genes. Most of them are involved in the tetrad wall and pollen outer wall exine during cell wall transition (Shi *et al.*, 2021; Zhu *et al.*, 2020). This study reveals that *OsTMS19* affects intine formation through ROS induced by temperature, providing a new perspective for understanding the mechanism of P/TGMS. For *tms5*, *ostms15* and *ostms18*, the genetic mutations are different. The defects for pollen development in the above mutants are also distinct. However, excessive ROS accumulation was detected in anther at stages 10–11 in these lines under high temperature (Figure 6). During these stages, the developing microspores undergo intine formation. Therefore, we propose that the accumulation of ROS under high temperature also affected the formation of intine in these P/TGMS lines.

Light and temperature affect P/TGMS fertility through the dual effects of ROS and slow development

Light and temperature play crucial roles in influencing the growth and development of plants. Plants grow under a certain range of light and temperature conditions. When exposed to low temperature or short-day conditions, the growth and development of plants can be slowed, along with a decrease in the ROS induced by the environment (Atkinson and Porter, 1996; Zhao *et al.*, 2018a,b; Zhu *et al.*, 2020). Studies conducted on Arabidopsis P/TGMS lines have revealed that slow development is a general mechanism that leads to fertility restoration in these lines (Zhang *et al.*, 2020; Zhu *et al.*, 2020). The present study establishes that fertility restoration in *ostms19* is primarily attributed to the reduction in ROS levels due to low temperature and a short-day photoperiod (Figure 8b). This mechanism could be applied to fertility regulation in other crops, as rice and other crops often face high-temperature and long-day photoperiod growth conditions. Combined with previous research, we propose that the P/TGMS mechanism involves both slow

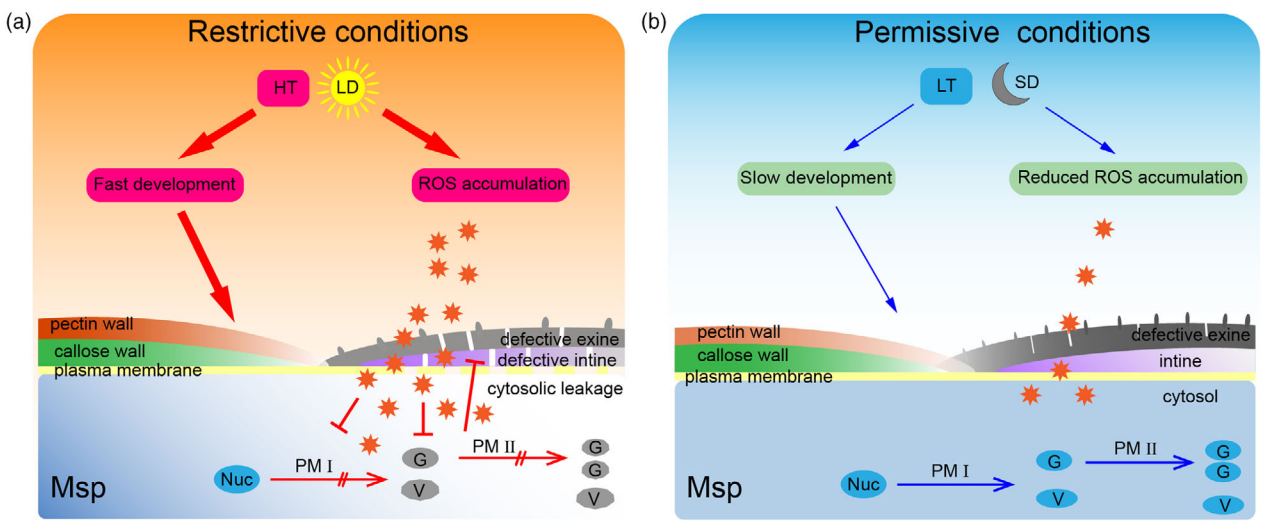

Figure 8 The mechanism of P/TGMS. During the 'transition period', the cell wall undergoes a tremendous change during pollen development. The tetrad wall (the pectin wall and the callose wall) is gradually degraded, and sporopollenin deposition begins outside of the microspore to form the exine. During stages 10–11, microspores undergo PM I and PM II and begin to synthesize the pollen intine wall. (a) Under high-temperature and long-day photoperiod conditions (HT: high temperature; and LD: long-day photoperiod), the microspores undergo faster development, with more accumulation of ROS. In the P/TGMS microspores, excessive ROS contents disrupt mitosis progress and lead to pollen abortion. (b) Under low-temperature or short-day photoperiod conditions (LT: low temperature and SD: short-day photoperiod), the development of microspores is slowed and naturally maintained at a low ROS level, which allows the microspores to form the intine layer and tide over the transition period in P/TGMS lines.

development and ROS homeostasis (Figure 8a,b). (i) The restoration of fertility in plant P/TGMS lines is a result of the combined influence of light and temperature, as both are essential for plant growth and development. (ii) Low temperature and short-day photoperiod not only slow plant growth and development but also reduce the accumulation of ROS. Therefore, the P/TGMS mechanism includes two aspects: slow development and ROS homeostasis. (iii) The essence of fertility restoration of P/TGMS lines is the formation of functional pollen. Light and temperature regulate the cell wall transition in P/TGMS lines through their impact on growth rate and ROS homeostasis, consequently affecting fertility (Figure 8). Rice typically grows under intense sunlight and high temperatures, while Arabidopsis is a shade plant that is typically cultivated indoors under lower light and temperature conditions. Therefore, the importance of slow development and ROS homeostasis for fertility restoration differs between the two species. Slow development plays a more crucial role in Arabidopsis, whereas ROS homeostasis has a more pronounced impact on fertility restoration in rice.

Materials and methods

Plant materials

The rice lines utilized in this study included the wild-type ZH11 (*Oryza sativa* ssp. japonica), *ostms19*, *tms5*, *ostms15* and *ostms18*, which were derived from an EMS mutagenized ZH11 library. These rice plants were cultivated in a paddy field located in Shanghai. Additionally, transgenic complementation lines, namely, *tms19-comp* and *tms19-gfp*, as well as CRISPR knockout plants, were grown at the Shanghai Normal University Botanical Garden.

Phenotypic analysis

We documented plant and spike phenotypes using a Nikon D7000 digital camera (Nikon, Japan). An Olympus SZX10 dissecting microscope (Olympus, Japan) was used to capture anther phenotypes. To visualize the I_2/KI staining results of pollen, we used an Olympus BX51 fluorescence microscope (Olympus, Japan). Pollen intine and exine were costained with basic fuchsin and fluorescent brightener-28 and subsequently examined using a laser confocal microscope FV3000 (Olympus, Japan), following the staining procedures outlined in (Jia *et al.*, 2021; Yang *et al.*, 2022). Cytological observations of anthers and pollen were conducted through semithin sectioning using an ultramicrotome (Leica, Germany), transmission electron microscopy (JEOL, Japan), and scanning electron microscopy (Hitachi, Japan). Further details of these analytical procedures can be found in previously published work (Han *et al.*, 2021).

BSA sequencing

To purify the mutant background and establish the F_2 sequencing population, *ostms19* and ZH11 underwent a series of hybridization processes. A comprehensive description of the BSA sequencing methodology was provided in a previous study (Zhang *et al.*, 2022).

Analysis of TGMS traits

Batches of *ostms19*, *tms5*, *ostms15* and *ostms18* seeds were germinated weekly from May to August (2020–2022). Once the seedlings attained a proper height, they were transplanted into the paddy field. The average temperature during the booting stage for each batch of plants was documented, and concurrently, the seed-setting rate was recorded. The assessment of TGMS traits in *ostms19* closely followed the methods outlined in a prior study (Zhang *et al.*, 2022).

Comet assay

Rice pollen grains were gathered, suspended in low-melting agarose, and evenly applied onto glass slides. Following agarose solidification, the slides were immersed in lysis and alkaline buffers to eliminate cell membranes and proteins from the pollen. Subsequently, electrophoresis was conducted for 10 min, and the DNA from disrupted nuclei migrated more rapidly than intact nuclear DNA. Staining with propidium iodide ensued, and analysis was conducted using a laser confocal microscope FV3000 (Olympus, Japan; Xue *et al.*, 2020). The images were analysed using the OpenComet plugin in the ImageJ to evaluate the percentage of DNA in each comet's tail (Tail DNA%: the percentage of DNA content in the tail compared to the total DNA content in the comet). We divided the extent of DNA damage into four groups based on the amount of Tail DNA: 1% (intact nucleus, little or no DNA in the tail), 1%–30% (1%–30% DNA in the tail), 30%–70% (30%–70% DNA in the tail), >70% (more than 70% DNA in the tail). Data from three slides were collected for each group, with 50 comet images captured per slide.

Detection of mitochondrial ETC activities

The activities of mitochondrial ETC complexes I, III, IV and V were measured using the mitochondrial complexes Activity Assay Kit according to the manufacturer's instructions (Solarbio, China).

ROS content determination

Anthers at different developmental stages of both ZH11 and *ostms19* were extracted from the husk, immersed in 10 mM potassium citrate buffer (pH 6.0) containing 0.5 mM nitroblue tetrazolium (NBT, Yeasen, China), and exposed to 5 min of vacuum treatment. Subsequently, the samples were incubated at 25 °C for 6 h to assess superoxide anion (O^{-2}) content and distribution (Hu *et al.*, 2011; Xie *et al.*, 2014). After NBT staining, the anthers underwent a decolorization process and were then embedded in paraffin. The relative content of ROS was determined through sectioning, and analysis was conducted using ImageJ. Hydrogen peroxide (H_2O_2) staining in anthers employed 2,7-dichlorodihydrofluorescein diacetate (H_2DCF-DA, Sigma–Aldrich). Anthers were immersed in a 5 μM H_2DCF-DA staining solution, exposed to 5 min of vacuum treatment, and subsequently incubated at 25 °C for 2–3 h. Following the removal of the staining solution, anther compression was carried out, and fluorescence was analysed using a laser confocal microscope (Wu *et al.*, 2023).

Immunohistochemistry

Panicles from both ZH11 and *ostms19-gfp* were immersed in FAA solution, subjected to a 15-min vacuum treatment, and fixed at 4 °C for 1–3 days. Dehydration and clearing of the samples were accomplished through a gradient of alcohol and xylene, followed by paraffin embedding. Sections with an 8 μm thickness were obtained using an MR2 rotary microtome (RMC). Deparaffinization and rehydration procedures were performed, and endogenous peroxidase activity was quenched by immersing slides in 3% H_2O_2 for 10 min. Antigen retrieval was conducted by placing slides in a boiled sodium citrate solution (0.01 M, pH = 6.0). Subsequently, the slides were blocked with 5% BSA for 30 min,

followed by incubation with a GFP antibody (Beyotime, China) (dilution 1 : 1000) and a secondary antibody (dilution 1 : 1000). Immunostaining was performed using the SABC-Kit and DAB (Beyotime, China).

In situ hybridization

Sections from ZH11 panicles embedded in blocks were precisely sliced to a thickness of 7 μm. A specific 350 bp fragment from the *OsTMS19* CDS was cloned and inserted into the pBluescript-SK vector (Stratagene). The vector underwent enzymatic cutting using *Bam*HI and *Eco*RI, and the products were utilized as transcription templates for generating sense and antisense probes. These probes were synthesized using T7 and T3 RNA polymerases and labelled with digoxigenin (Roche, Switzerland). The detailed procedures for RNA hybridization and immunodetection were outlined in a previous study (Han *et al*., 2021; Zhu *et al*., 2011).

Expression analysis

Total RNA was extracted from anthers at different stages of ZH11 using the TRIzol reagent kit (Invitrogen, Waltham, USA). cDNA was reverse-transcribed with TransScript Fly First-Strand cDNA Synthesis SuperMix (TransGen Biotech, China). SYBR Green Real-time PCR Master Mix (Toyobo, Japan) and the ABI 7300 system (Life Technologies, Carlsbad, CA, USA) were employed for qRT–PCR analysis, as previously described (Han *et al*., 2021). The internal reference gene utilized was OsACTIN, and each experiment was conducted with three biological replicates.

Subcellular localization

The full-length cDNA of *OsTMS19* was cloned and inserted into the pCAMBIA1300 vector driven by the 35S promoter to construct the TMS19-GFP fusion protein. Rice protoplasts were prepared, and 10 μL of plasmid was added to 100 μL of protoplast suspension, followed by incubation in the dark for 12–16 h. MitoTracker Red CMXRos (Invitrogen) was used as a mitochondrial marker. The protoplasts were stained for 10–15 min, and fluorescence was observed using a laser confocal microscope FV3000 (Olympus, Japan).

Phylogenetic analysis

The complete protein sequence of OsTMS19 was used as the query in a Basic Local Alignment Search Tool search conducted on the National Center for Biotechnology Information website (http://www.ncbi.nlm.nih.gov/). The resulting homologous sequences were aligned using the Clustal W tool for multiple sequence alignment. Phylogenetic trees were then constructed and validated by MEGAX with the neighbour-joining method.

Acknowledgements

This work was supported by grants from the National Key R&D Program of China (2022YFF1003502), the National Science Foundation of China (31930009, 32070343), the Innovation Program of Shanghai Municipal Education Commission (2019-01-07-00-02-E00006) and Jiangxi Provincial Natural Science Foundation (20232BAB215002).

Author contributions

The project leader: Z.-N.Y. Conceived the study: Z.-N.Y. and J.Z. Phenotype and cytological analysis: L.Z. and Y.-M.Y. Expression analysis: L.Z. and J.-J.W. Vector construction: L.Z., Y.-M.Y. and X.Z. Mutant screening and sequencing populations construction: L.Z., Q.-S.S., Y.H. and Y.-F.Z. ROS measurement and comet assay: L.Z. and Y.-C.M. BSA-seq analysis: X.-H.H. Writing-original draft: Z.-N.Y., J.Z. and L.Z. Writing review & editing: Z.-N.Y. and B.M. All authors read and approved the manuscript.

Data availability statement

Data sharing not applicable to this article as no datasets were generated or analysed during the current study.

References

Atkinson, D. and Porter, J.R. (1996) Temperature, plant development and crop yields. *Trends Plant Sci.* **1**, 119–124.

Bai, S., Yu, H., Wang, B. and Li, J. (2018) Retrospective and perspective of rice breeding in China. *J. Genet. Genomics*, **45**, 603–612.

Canino, G., Bocian, E., Barbezier, N., Echeverría, M., Forner, J., Binder, S. and Marchfelder, A. (2009) Arabidopsis encodes four tRNase Z enzymes. *Plant Physiol.* **150**, 1494–1502.

Chaturvedi, P., Wiese, A.J., Ghatak, A., Záveská Drábková, L., Weckwerth, W. and Honys, D. (2021) Heat stress response mechanisms in pollen development. *New Phytol.* **231**, 571–585.

Chen, L. and Liu, Y.G. (2014) Male sterility and fertility restoration in crops. *Annu. Rev. Plant Biol.* **65**, 579–606.

Chen, R., Zhao, X., Shao, Z., Wei, Z., Wang, Y., Zhu, L., Zhao, J. *et al*. (2007) Rice UDP-glucose pyrophosphorylase1 is essential for pollen callose deposition and its cosuppression results in a new type of thermosensitive genic male sterility. *Plant Cell*, **19**, 847–861.

Chen, G., Zou, Y., Hu, J. and Ding, Y. (2018) Genome-wide analysis of the rice PPR gene family and their expression profiles under different stress treatments. *BMC Genomics*, **19**, 720.

Colcombet, J., Lopez-Obando, M., Heurtevin, L., Bernard, C., Martin, K., Berthomé, R. and Lurin, C. (2013) Systematic study of subcellular localization of Arabidopsis PPR proteins confirms a massive targeting to organelles. *RNA Biol.* **10**, 1557–1575.

Ding, J., Lu, Q., Ouyang, Y., Mao, H., Zhang, P., Yao, J., Xu, C. *et al*. (2012) A long noncoding RNA regulates photoperiod-sensitive male sterility, an essential component of hybrid rice. *Proc. Natl Acad. Sci. USA*, **109**, 2654–2659.

Dong, X., Hong, Z., Sivaramakrishnan, M., Mahfouz, M. and Verma, D.P. (2005) Callose synthase (CalS5) is required for exine formation during microgametogenesis and for pollen viability in Arabidopsis. *Plant J.* **42**, 315–328.

Fan, Y. and Zhang, Q. (2018) Genetic and molecular characterization of photoperiod and thermo-sensitive male sterility in rice. *Plant Reprod.* **31**, 3–14.

Fan, Y., Yang, J., Mathioni, S.M., Yu, J., Shen, J., Yang, X., Wang, L. *et al*. (2016) PMS1T, producing phased small-interfering RNAs, regulates photoperiod-sensitive male sterility in rice. *Proc. Natl Acad. Sci. USA*, **113**, 15144–15149.

Gechev, T.S., Van Breusegem, F., Stone, J.M., Denev, I. and Laloi, C. (2006) Reactive oxygen species as signals that modulate plant stress responses and programmed cell death. *Bioessays*, **28**, 1091–1101.

Han, Y., Zhou, S.D., Fan, J.J., Zhou, L., Shi, Q.S., Zhang, Y.F., Liu, X.L. *et al*. (2021) OsMS188 is a key regulator of tapetum development and sporopollenin synthesis in rice. *Rice*, **14**, 4.

Han, Y., Jiang, S.Z., Zhong, X., Chen, X., Ma, C.K., Yang, Y.M., Mao, Y.C. *et al*. (2023) Low temperature compensates for defective tapetum initiation to restore the fertility of the novel TGMS line ostms15. *Plant Biotechnol. J.* **21**, 1659–1670.

Hu, L., Liang, W., Yin, C., Cui, X., Zong, J., Wang, X., Hu, J. *et al*. (2011) Rice MADS3 regulates ROS homeostasis during late anther development. *Plant Cell*, **23**, 515–533.

Hu, Z.X., Tian, Y. and Xu, Q.S. (2016) Review of extension and analysis on current status of hybrid rice in China. *Hybrid Rice*, **31**, 1–8.

Jia, X.L., Xue, J.S., Zhang, F., Yao, C., Shen, S.Y., Sui, C.X., Peng, Y.J. *et al*. (2021) A dye combination for the staining of pollen coat and pollen wall. *Plant Reprod.* **34**, 91–101.

Jiang, C., Sun, J., Li, R., Yan, S., Chen, W., Guo, L., Qin, G. *et al*. (2022) A reactive oxygen species burst causes haploid induction in maize. *Mol. Plant*, **15**, 943–955.

Mittler, R., Vanderauwera, S., Gollery, M. and Van Breusegem, F. (2004) Reactive oxygen gene network of plants. *Trends Plant Sci.* **9**, 490–498.

Peng, G., Liu, M., Zhu, L., Luo, W., Wang, Q., Wang, M., Chen, H. *et al*. (2023) The E3 ubiquitin ligase CSIT1 regulates critical sterility-inducing temperature by ribosome-associated quality control to safeguard two-line hybrid breeding in rice. *Mol. Plant*, **16**, 1695–1709.

Peng, G., Liu, M., Luo, Z., Deng, S., Wang, Q., Wang, M., Chen, H. *et al*. (2024) An E3 ubiquitin ligase CSIT2 controls critical sterility-inducing temperature of thermo-sensitive genic male sterile rice. *New Phytol.* **241**, 2059–2074.

Shi, Q.S., Lou, Y., Shen, S.Y., Wang, S.H., Zhou, L., Wang, J.J., Liu, X.L. *et al*. (2021) A cellular mechanism underlying the restoration of thermo/photoperiod-sensitive genic male sterility. *Mol. Plant*, **14**, 2104–2114.

Si, H.M., Liu, W.Z., Fu, Y.P., Sun, Z.X. and Hu, G.C. (2011) Current situation and suggestions for development of two-line hybrid rice in China. *Chin. J. Rice Sci.* **25**, 544–552.

Tester, M. and Langridge, P. (2010) Breeding technologies to increase crop production in a changing world. *Science*, **327**, 818–822.

Wan, C., Li, S., Wen, L., Kong, J., Wang, K. and Zhu, Y. (2007) Damage of oxidative stress on mitochondria during microspores development in Honglian CMS line of rice. *Plant Cell Rep.* **26**, 373–382.

Wang, K.Q., Yu, Y.H., Jia, X.L., Zhou, S.D., Zhang, F., Zhao, X., Zhai, M.Y. *et al*. (2022) Delayed callose degradation restores the fertility of multiple P/TGMS lines in Arabidopsis. *J. Integr. Plant Biol.* **64**, 717–730.

Waszczak, C., Carmody, M. and Kangasjärvi, J. (2018) Reactive oxygen species in plant signaling. *Annu. Rev. Plant Biol.* **69**, 209–236.

Willekens, H., Chamnongpol, S., Davey, M., Schraudner, M., Langebartels, C., Van Montagu, M., Inzé, D. *et al*. (1997) Catalase is a sink for H_2O_2 and is indispensable for stress defence in C3 plants. *EMBO J.* **16**, 4806–4816.

Wu, L., Jing, X., Zhang, B., Chen, S., Xu, R., Duan, P., Zou, D. *et al*. (2022) A natural allele of OsMS1 responds to temperature changes and confers thermosensitive genic male sterility. *Nat. Commun.* **13**, 2055.

Wu, S.Y., Hou, L.L., Zhu, J., Wang, Y.C., Zheng, Y.L., Hou, J.Q., Yang, Z.N. *et al*. (2023) Ascorbic acid-mediated reactive oxygen species homeostasis modulates the switch from tapetal cell division to cell differentiation in Arabidopsis. *Plant Cell* **35**, 1474–1495.

Wu, X.N., Li, J.Y., He, Q., Li, B.Q., He, Y.H., Pan, X., Wang, M.Y. *et al*. (2024) Targeting the PHF8/YY1 axis suppresses cancer cell growth through modulation of ROS. *Proc. Natl Acad. Sci. USA*, **121**, e2219352120.

Xie, H.T., Wan, Z.Y., Li, S. and Zhang, Y. (2014) Spatiotemporal production of reactive oxygen species by NADPH oxidase is critical for tapetal programmed cell death and pollen development in Arabidopsis. *Plant Cell*, **26**, 2007–2023.

Xie, D.L., Zheng, X.L., Zhou, C.Y., Kanwar, M.K. and Zhou, J. (2022) Functions of redox signaling in pollen development and stress response. *Antioxidants*, **11**, 287.

Xu, X.F., Qian, X.X., Wang, K.Q., Yu, Y.H., Guo, Y.Y., Zhao, X. and Yang, Z.N. (2021) Slowing development facilitates Arabidopsis mgt mutants to accumulate enough magnesium for pollen formation and fertility restoration. *Front. Plant Sci.* **11**, 621338.

Xue, J.S., Zhang, B., Zhan, H., Lv, Y.L., Jia, X.L., Wang, T., Yang, N.Y. *et al*. (2020) Phenylpropanoid derivatives are essential components of sporopollenin in vascular plants. *Mol. Plant*, **13**, 1644–1653.

Yang, N.Y., Jia, X.L., Sui, C.X., Shen, S.Y., Dai, X.L., Xue, J.S. and Yang, Z.N. (2022) Documenting the sporangium development of the polypodiales fern Pteris multifida. *Front. Plant Sci.* **13**, 878693.

Yao, X.Z., Hu, W. and Yang, Z.N. (2022) The contributions of sporophytic tapetum to pollen formation. *Seed Biol.* **1**, 5–13.

Yu, J., Han, J., Kim, Y.J., Song, M., Yang, Z., He, Y., Fu, R. *et al*. (2017) Two rice receptor-like kinases maintain male fertility under changing temperatures. *Proc. Natl Acad. Sci. USA*, **114**, 12327–12332.

Yuan, L.P. (2014) Development of hybrid rice to ensure food security. *Rice Sci.* **21**, 1–2.

Zhang, D., Luo, X. and Zhu, L. (2011) Cytological analysis and genetic control of rice anther development. *J. Genet. Genomics*, **38**, 379–390.

Zhang, C., Xu, T., Ren, M.Y., Zhu, J., Shi, Q.S., Zhang, Y.F., Qi, Y.W. *et al*. (2020) Slow development restores the fertility of photoperiod-sensitive male-sterile plant lines. *Plant Physiol.* **184**, 923–932.

Zhang, Y.F., Li, Y.L., Zhong, X., Wang, J.J., Zhou, L., Han, Y., Li, D.D. *et al*. (2022) Mutation of glucose-methanol-choline oxidoreductase leads to thermosensitive genic male sterility in rice and Arabidopsis. *Plant Biotechnol. J.* **20**, 2023–2035.

Zhao, Q., Zhou, L., Liu, J., Cao, Z., Du, X., Huang, F. and Cheng, F. (2018a) Involvement of CAT in the detoxification of HT-induced ROS burst in rice anther and its relation to pollen fertility. *Plant Cell Rep.* **37**, 741–757.

Zhao, Q., Zhou, L., Liu, J., Du, X., Asad, M.A., Huang, F., Pan, G. *et al*. (2018b) Relationship of ROS accumulation and superoxide dismutase isozymes in developing anther with floret fertility of rice under heat stress. *Plant Physiol. Biochem.* **122**, 90–101.

Zheng, S., Li, J., Ma, L., Wang, H., Zhou, H., Ni, E., Jiang, D. *et al*. (2019) OsAGO2 controls ROS production and the initiation of tapetal PCD by epigenetically regulating OsHXK1 expression in rice anthers. *Proc. Natl Acad. Sci. USA*, **116**, 7549–7558.

Zhou, H., Liu, Q., Li, J., Jiang, D., Zhou, L., Wu, P., Lu, S. *et al*. (2012) Photoperiod- and thermo-sensitive genic male sterility in rice are caused by a point mutation in a novel noncoding RNA that produces a small RNA. *Cell Res.* **22**, 649–660.

Zhou, H., Zhou, M., Yang, Y., Li, J., Zhu, L., Jiang, D., Dong, J. *et al*. (2014) RNase Z(S1) processes UbL40 mRNAs and controls thermosensitive genic male sterility in rice. *Nat. Commun.* **5**, 4884.

Zhu, J., Lou, Y., Shi, Q.S., Zhang, S., Zhou, W.T., Yang, J., Zhang, C. *et al*. (2020) Slowing development restores the fertility of thermo-sensitive male-sterile plant lines. *Nat. Plants*, **6**, 360–367.

Zhu, J., Lou, Y., Xu, X. and Yang, Z.N. (2011) A genetic pathway for tapetum development and function in Arabidopsis. *J. Integr. Plant Biol.* **53**, 892–900.

Supporting information

Additional supporting information may be found online in the Supporting Information section at the end of the article.

Figure S1 The plant phenotype of *ostms19-gfp*.
Figure S2 Statistical analysis of plants height of ZH11 and *ostms19*.
Figure S3 The phylogenetic tree of OsTMS19.
Figure S4 SEM observation for the pollen grains of ZH11 and *ostms19*.
Figure S5 statistical analysis of different defective types.
Figure S6 Cytological analysis of pollen development in ZH11 and *ostms19*.
Table S1 List of primers used in the study and their sequences

